Few-Body Syst (2023) 64:14
https://doi.org/10.1007/s00601-023-01798-w

Julien Gibelin

On the Experimental Description of Neutron Resonances

Received: 13 March 2023 / Accepted: 14 March 2023 / Published online: 30 March 2023

Abstract We present a collection of simple derivations for the neutron-induced resonance cross-sections. These formulae are commonly used to experimentally describe the fundamental properties of resonances for neutron-rich nuclei far from stability and to describe unbound nuclei. The main goal of this article is to illustrate their dependencies with basic observables in order to discuss the pertinence of experimental approaches in the derivation of their properties, especially for "N-body" resonances.

1 Introduction

The advent of new generation radioactive beam facilities has provided the ability of experimentally measuring resonances far from the valley of stability, and in particular on the neutron-rich side. It also allows neutron unbound nuclei to be produced and studied, and their fundamental characteristics to be deduced. Physicists widely use a set of simple formulae to extract their properties. However theses equations have intrinsic limitations than can lead to misunderstanding when they are compared with their theoretical description. We present in the following sections a simple approach for their derivation, keeping their expression dependent on only simple tabulated functions. We then illustrate and discuss their behavior with experimentally accessible observables and parameters.

2 Derivation of the Main Equations

2.1 Scattering Cross-Section

As we will see later, describing neutron states in the continuum and in particular unbound (neutron-rich) nuclei, comes down at first order to describing the resonant scattering of a neutron on a nucleus (Fig. 1).

If a priori we should consider a dynamical evolution of the wave packet describing the diffusion of the neutron on the nuclear potential of the nucleus of interest, we can show that the size of the corresponding wave packet is large enough to be decomposed into standing waves [1].

A large part of the formalisms and derivations presented below come from the books of Blatt and Weisskopf [2] or Satchler [3] as well as from the R-matrix formalism [4,5].

We can represent the incident beam (here the neutron) by a plane wave:

$$\exp(i\vec{k}\vec{r}) = \exp(ikz) \tag{1}$$

J. Gibelin (✉)
Université de Caen Normandie, ENSICAEN, CNRS/IN2P3, LPC Caen UMR6534, 14000 Caen, France
E-mail: gibelin@unicaen.fr

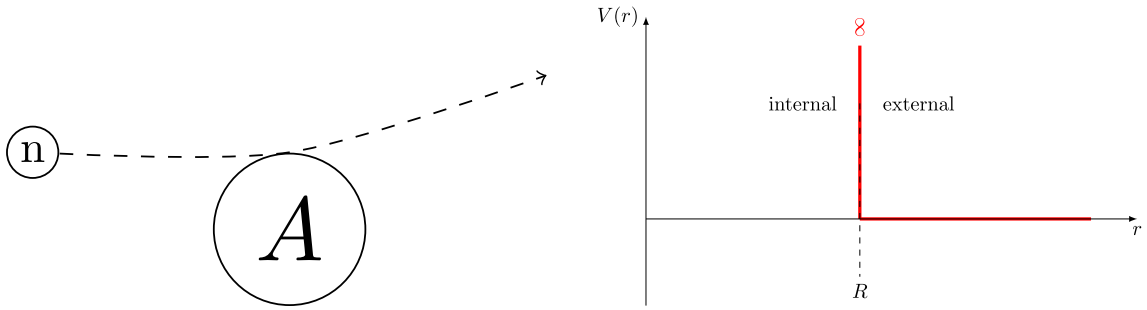

Fig. 1 Schematic (left) and potential (right) of the reaction considered here

the wave number being calculated from the energy E of the system fragment plus neutron:

$$\vec{k} = \frac{\mu\vec{v}}{\hbar} \Rightarrow k = \frac{\sqrt{2\mu E}}{\hbar} \qquad \text{with} \qquad \mu = \frac{M_{frag}M_n}{M_{frag}+M_n} \tag{2}$$

We develop this plane wave on the basis of spherical harmonics $\mathcal{Y}_{\ell,m}(\theta)$, taking into account that we have a cylindrical symmetric problem and that only the harmonics with $m = 0$ come into play:

$$\begin{aligned} \exp(ikz) &= \sum_{\ell=0}^{\infty} \mathcal{A}_\ell(r)\mathcal{Y}_{\ell,0}(\theta) \\ \text{with } \mathcal{A}_l(r) &= \int \mathcal{Y}^*_{\ell,0}(\theta)\exp\left(ikr\cos\theta\right)d\Omega = i^\ell\sqrt{4\pi(2\ell+1)}\,j_\ell(kr) \end{aligned} \tag{3}$$

and j_p the spherical Bessel function of first kind and order p. The expression of the latter simplifies at large distances (here $kr \gg \ell$): $j_p(x) \to \frac{\sin(x-\frac{p\pi}{2})}{x}$ and by recalling that $\sin(x) = \frac{e^{ix}-e^{-ix}}{2i}$, we get:

$$\exp(ikz) \approx \frac{\sqrt{\pi}}{kr}\sum_{\ell=0}^{\infty}\sqrt{2\ell+1}\,i^{\ell+1}\Big\{\underbrace{\exp\left[-i\,\left(kr-\frac{\pi}{2}\ell\right)\right]}_{\text{incoming wave}} \underbrace{-\exp\left[+i\,\left(kr-\frac{\pi}{2}\ell\right)\right]}_{\text{outgoing wave}}\Big\}\mathcal{Y}_{\ell,0} \tag{4}$$

However, this expression describes an unperturbed wave. As we are trying to describe the scattering of this wave on the nuclear potential of the fragment, we have to modify this expression for the outgoing wave, by allowing the latter to be scaled by a complex factor η_ℓ:

$$\psi\left(\vec{r}\right) = \frac{\sqrt{\pi}}{kr}\sum_{\ell=0}^{\infty}\sqrt{2\ell+1}\,i^{\ell+1}\Big\{\underbrace{\exp\left[-i\left(kr-\frac{\pi}{2}\ell\right)\right]}_{\text{incoming wave}} \underbrace{-\eta_\ell\exp\left[+i\left(kr-\frac{\pi}{2}\ell\right)\right]}_{\text{outgoing wave}}\Big\}\mathcal{Y}_{\ell,0} \tag{5}$$

The scattered wave is then obtained by $\psi_{\text{sc}} = \psi - \exp(ikz)$, whose integration of the flux gives the scattering cross-section:

$$\sigma_{sc,\ell} = \pi\lambda\!\!\!^{-2}\,(2\ell+1)\,\|1-\eta_\ell\|^2 \tag{6}$$

The integration of the flux of the total wave function ψ allows us to deduce the expression of the reaction cross-section:

$$\sigma_{r,\ell} = \pi\lambda\!\!\!^{-2}\,(2\ell+1)\left(1-\|\eta_\ell\|^2\right) \tag{7}$$

A cross-section being necessarily positive, the expression of $\sigma_{r,\ell}$ implies $\|\eta_\ell\| \leq 1$.

2.2 Expression of Energy Shift and Penetrability

Let us now address the reaction of interest. The radial Schrödinger equation gives:

$$\frac{d^2u_\ell}{dr^2} + \left[k^2 - \frac{\ell\,(\ell+1)}{r^2} - \frac{2\mu}{\hbar^2}V(r)\right]u_\ell = 0 \tag{8}$$

with μ the reduced mass of the system and $V(r)$ the Coulomb potential. Within the hard sphere approximation, and since neutrons are uncharged, $V(r) = 0$ for $r > R$. We can thus write outside the nucleus:

$$\frac{d^2u_\ell}{dr^2} + \left[k^2 - \frac{\ell\,(\ell+1)}{r^2}\right]u_\ell = 0 \tag{9}$$

With the so-called *regular* (which goes to 0 when r goes to 0) and *irregular* solutions, respectively noted $F_\ell(r)$ and $G_\ell(r)$[1], written:

$$F_\ell(r) = \sqrt{\frac{\pi kr}{2}}J_{\ell+1/2}\,(kr) \tag{10}$$

$$G_\ell(r) = -\sqrt{\frac{\pi kr}{2}}Y_{\ell+1/2}\,(kr) = (-1)^\ell\sqrt{\frac{\pi kr}{2}}J_{-(\ell+1/2)}\,(kr) \tag{11}$$

where J_p and Y_p are the Bessel functions of order p, respectively of first and second kind.

We then have:

$$-\text{ incoming term:}\quad u_\ell^{(+)} = G_\ell(r) + i\,F_\ell(r) = \sqrt{\frac{\pi kr}{2}}H^{(2)}_{\ell+1/2}(kr) \tag{12}$$

$$-\text{ outgoing term:}\quad u_\ell^{(-)} = \overline{u}_\ell^{(+)} = \sqrt{\frac{\pi kr}{2}}H^{(1)}_{\ell+1/2}(kr) \tag{13}$$

with $H_p^{(1,2)}(z)$ the Hankel functions of order p, of the first and second kind. Outside the nucleus, the radial part of the wave function is a linear combination of the incoming and outgoing terms:

$$u_\ell = \alpha\,u_\ell^{(+)} + \beta\,u_\ell^{(-)} \tag{14}$$

As at large distances the wave function must converge to the shape found in (5):

$$\lim_{r\to\infty} u_\ell = \frac{\sqrt{\pi}}{kr}\sqrt{2\ell+1}\,i^{\ell+1}\left\{\exp\left[-i\left(kr - \frac{\pi}{2}\ell\right)\right] - \eta_\ell\exp\left[+i\left(kr - \frac{\pi}{2}\ell\right)\right]\right\} \tag{15}$$

By recalling that the asymptotic forms of the Hankel functions are:

$$H_p^1(z) \to \sqrt{\frac{2}{\pi z}}\exp\left[+i\left(z - \frac{p\pi}{2} - \frac{\pi}{4}\right)\right] \text{ and } H_p^2(z) \to \sqrt{\frac{2}{\pi z}}\exp\left[-i\left(z - \frac{p\pi}{2} - \frac{\pi}{4}\right)\right]$$

this implies:

$$\lim_{r\to\infty} u_\ell^{(+)} = +i\ \exp\left[-i\left(kr - \frac{\pi}{2}\ell\right)\right] \tag{16}$$

$$\lim_{r\to\infty} u_\ell^{(-)} = -i\ \exp\left[+i\left(kr - \frac{\pi}{2}\ell\right)\right] \tag{17}$$

and thus we have:

$$\alpha = i\sqrt{2+1}\frac{\sqrt{\pi}}{kr} \tag{18}$$

$$\beta = -\eta_\ell\,\alpha \tag{19}$$

[1] Riccati-Bessel functions, solutions of the differential equation $x^2\frac{d^2y}{dx^2} + \left[x^2 - n(n+1)\right]y = 0$. To get back to the present problem simply put $n = \ell$, $x = kr$ and $y = u_\ell\,(kr)$.

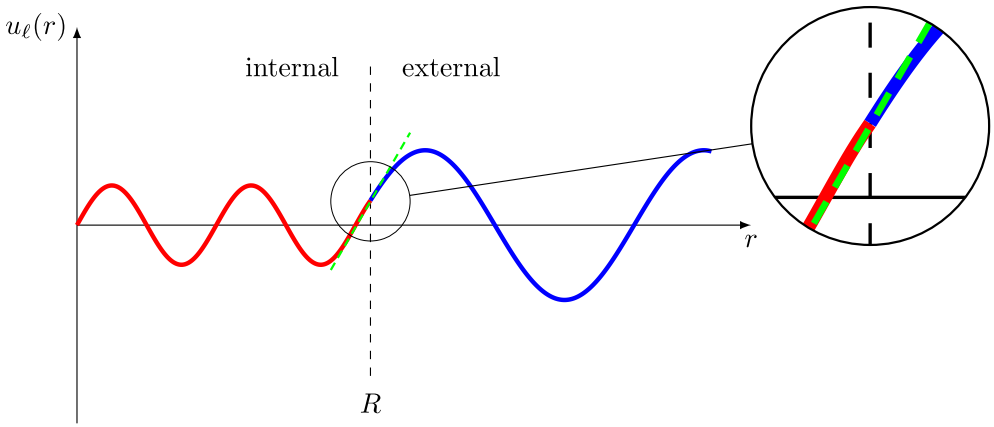

Fig. 2 Schematic representation of the radial wave function, separating the inner (red) and outer part (blue)

The value of η_ℓ is connected to the conditions of continuity at the surface (see a schematics representation in Fig. 2). To calculate these conditions, we define f_ℓ, the logarithmic derivative of the radial part of the wave function at the surface:

$$f_\ell = R\left[\frac{du_\ell/dr}{u_\ell}\right]_{r=R} \tag{20}$$

For the part outside the core, we can define:

$$R\left[\frac{du_\ell^{(+)}/dr}{u_\ell^{(+)}}\right]_{r=R} = \Delta_\ell + is_\ell \tag{21}$$

with Δ_ℓ and s_ℓ real, which correspond to the energy shift and the penetrability:

$$\Delta_\ell = R\ v_\ell\ \left[G_\ell(R)\ G'_\ell(R) + F_\ell(R)\ F'_\ell(R)\right] \tag{22}$$

$$s_\ell = R\ v_\ell\ \left[G_\ell(R)\ F'_\ell(R) - F_\ell(R)\ G'_\ell(R)\right] = kRv_\ell \tag{23}$$

F', G' being the derivatives of F, G and:

$$v_\ell = \frac{1}{G_\ell^2\,(R) + F_\ell^2\,(R)} = \frac{2/\pi kR}{J^2_{\ell+1/2}(kR) + Y^2_{\ell+1/2}(kR)} \tag{24}$$

the penetrability factor itself. As its name indicates v_ℓ is a measure of how much the neutron penetrates the nucleus. So $v_\ell \ll 1$ means that the neutron does not penetrate enough, resulting in a weak interaction.

We define the phase shift ξ_ℓ as:

$$\exp\left(2i\xi_\ell\right) = \frac{u_\ell^{(+)}(R)}{u_\ell^{(-)}(R)} = \frac{G_\ell(R) - iF_\ell(R)}{G_\ell(R) + iF_\ell(R)} \tag{25}$$

Finally we can write the link between η_ℓ and f_ℓ, which gives after some rearrangements:

$$\eta_\ell = \frac{f_\ell - \Delta_\ell + is_\ell}{f_\ell - \Delta_\ell - is_\ell}\exp\left(2i\xi_\ell\right) \tag{26}$$

The Eqs. (6) and (7) then provide the scattering and reaction cross-sections:

$$\sigma_{sc,\ell} = (2\ell+1)\pi\lambda\!\!\!^{-2}\left\|A^\ell_{\text{res}} + A^\ell_{\text{pot}}\right\|^2 \tag{27}$$

$$\text{with } A^\ell_{\text{res}} = \frac{-2\ i\ s_\ell}{(\Re(f_\ell) - \Delta_\ell) + i\ (\Im(f_\ell) - s_\ell)} \tag{28}$$

$$A^\ell_{pot} = \exp\left(-2i\xi_\ell\right) - 1 \tag{29}$$

amplitudes for the internal "scattering" (i.e. resonance) and for the external potential. And:

$$\sigma_{r,\ell} = (2\ell+1)\pi\lambda\!\!\!^{-2}\frac{-4\ s_\ell\ \Im(f_\ell)}{(\Re(f_\ell)-\Delta_\ell)^2+(\Im(f_\ell)-s_\ell)^2} \tag{30}$$

In these equations, only the expression of f_ℓ is missing to compute the cross-sections, which we will do later with some approximations. We can nevertheless conclude here, from (30), that f_ℓ must be zero or negative. Since s_ℓ appears in the numerator, the reaction cross-section follows the evolution of the penetrability. Finally, by looking only at the resonant part of the diffusion (A^ℓ_{res}) we find that for given s_ℓ and Δ_ℓ, the amplitude is more important as f_ℓ is low.

2.3 Expression of the Shape of a Resonance

The main idea, given the results obtained previously, is to find an expression of f_ℓ showing its energy dependence. We will assume that we have purely a resonance and that the input channel of the reaction is equal to the output channel (resonant elastic scattering). Knowing that f_ℓ is the derivative of u_ℓ we have to find an expression of the latter.

Just inside the core ($r \leq R$) we can write, by definition of the phase shift (25):

$$u_\ell(r) \sim \exp(-ikr) + \exp(ikr + 2i\xi_\ell) = 2\ \exp(i\xi_\ell)\ \cos(kr+\xi_\ell) \tag{31}$$

We have therefore for its derivative, evaluated in R:

$$u'_\ell(R) \sim -2\ \exp(i\xi_\ell)\ k\ \sin(kR+\xi_\ell) \tag{32}$$

and consequently:

$$f_\ell(R) = R\frac{u'_\ell(R)}{u_\ell(R)} \sim -kR\tan(kR+\xi_\ell) \tag{33}$$

Recalling that ξ_ℓ depends a priori on energy, this function will alternate in energy between two poles and zero values. This last value maximizes a priori the amplitude of the resonant scattering (Eq. (28)).

We can therefore expand f_ℓ around the resonance energy E_0:

$$f_\ell(E) = (E-E_0)\underbrace{\left[\frac{df_\ell(E)}{dE}\right]_{E=E_0}}_{f'(E_0)} + \dots \tag{34}$$

The expression for the amplitude (28) becomes:

$$A^\ell_{\text{res}} = \frac{-2\ i\ s_\ell}{[(E-E_0)\ f'(E_0)-\Delta_\ell]-i\ s_\ell} \tag{35}$$

which can be rewritten:

$$A^\ell_{res} = \frac{i\ \Gamma}{(E-E_0-\Delta E)+i\frac{1}{2}\Gamma} \tag{36}$$

$$\text{with} \quad \gamma^2 = -1/f'(E_0) \tag{37}$$

$$\Gamma = 2s_\ell\gamma^2 \tag{38}$$

$$\Delta E = \gamma^2\Delta_\ell \tag{39}$$

The quadratic norm of this amplitude, directly related to the cross-section, has the well-known form of a dispersion described by Breit & Wigner:

$$\left\| A^\ell_{\text{res}} \right\|^2 = \frac{\Gamma^2}{\left(E-E'_0\right)^2+\frac{1}{4}\Gamma^2} \tag{40}$$

where the energy $E'_0 = E_0 - \Delta E$ is the energy of the resonance shifted by a factor ΔE.

For a concise development of the equations presented here we can refer the reader for example to F. Gunsing's lectures at Joliot-Curie School 2014 [6].

2.4 Expression of the Energy-Dependent Apparent Width and Position of the Resonant State

We start from the characteristic expression of the cross-section distribution as deduced in the previous section:

$$\frac{d\sigma}{dE} \propto \frac{\Gamma_\ell\left(E\right)}{\left(E_0' - E\right)^2 + \frac{1}{4}\Gamma_\ell^2\left(E\right)} \tag{41}$$

The expression of the width and the energy shift are valid whatever E is, so in particular for E_0

$$\Gamma_\ell\left(E_0\right) = 2s_\ell\left(E_0\right)\gamma^2 = \Gamma_0 \tag{42}$$

the reduced width γ being constructed to be constant in energy we can write:

$$\frac{\Gamma_\ell\left(E\right)}{\Gamma_\ell\left(E_0\right)} = \frac{\Gamma_\ell\left(E\right)}{\Gamma_0} = \frac{s_\ell\left(E\right)}{s_\ell\left(E_0\right)} \tag{43}$$

and finally by developing the penetrability expression $s_\ell\left(E\right)$:

$$\Gamma_\ell\left(E\right) = \Gamma_0 \frac{k}{k_0} \frac{J_{\ell+1/2}^2(k_0R) + Y_{\ell+1/2}^2(k_0R)}{J_{\ell+1/2}^2(kR) + Y_{\ell+1/2}^2(kR)} \tag{44}$$

And in the same way for the energy shift:

$$\Delta E = -\left(s_\ell - B\right)\gamma^2 \tag{45}$$

Equation (42) allows us to extract the reduced width $\gamma^2 = \Gamma_0/(2s_\ell\left(E_0\right))$ which we reinject:

$$\Delta E = -\Gamma_0 \frac{s_\ell\left(E\right) - B}{2s_\ell\left(E_0\right)} \tag{46}$$

B is a constant that we choose such that at the energy of the resonance the shift is equal to zero, i.e. $B = s_\ell\left(E_0\right)$ and thus:

$$\Delta E = -\Gamma_0 \frac{s_\ell\left(E\right) - s_\ell\left(E_0\right)}{2s_\ell\left(E_0\right)} \tag{47}$$

as for $s_\ell\left(E\right)$ its expression:

$$s_\ell\left(E\right) = R\, v_\ell \left[G_\ell(R)\, G_\ell'(R) + F_\ell(R)\, F_\ell'(R)\right] \tag{48}$$

can be written, using the different properties of the Bessel functions:

$$\begin{aligned} s_\ell\left(E\right) = & \frac{-\ell}{J_{\ell+1/2}^2\left(kR\right) + Y_{\ell+1/2}^2\left(kR\right)} \\ & \left\{\left[J_{\ell+1/2}^2\left(kR\right)\ell + Y_{\ell+1/2}^2\left(kR\right)\right]\right. \\ & \left. -kR\left[J_{\ell+1/2}\left(kR\right)J_{\ell-1/2}\left(kR\right) + Y_{\ell+1/2}\left(kR\right)Y_{\ell-1/2}\left(kR\right)\right]\right\} \end{aligned} \tag{49}$$

The forms of the Eqs. (49) and (44) are therefore simple enough to be implemented in a computer code (there are many libraries for Bessel functions, for example the GSL [7]). In particular their expression is general whatever ℓ is, allowing to study the dependence in ℓ as an additional parameter, possibly without any prior hypothesis.

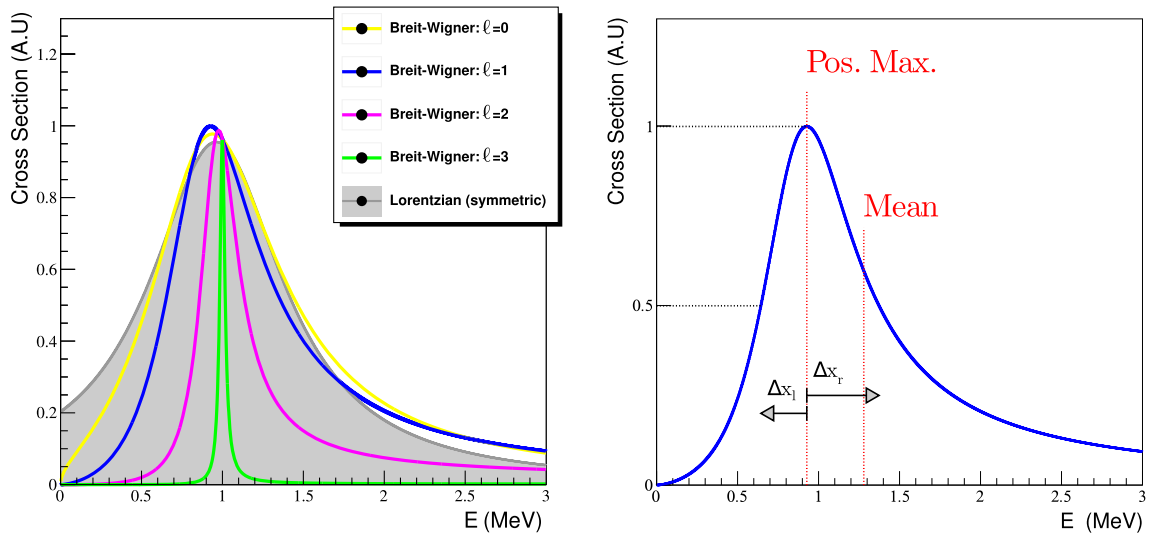

Fig. 3 Left: Lorentzian (grey) distribution compared to Breit-Wigner distributions with energy and ℓ dependent widths, taking into account the energy shift. For all curves $E_0 = \Gamma_0 = 1\,\text{MeV}$, only $\ell = 0, 1, 2$ and 3 (respectively yellow, blue, magenta and green) change. We assume here a $^{17}\text{B} + n$ system. Right: illustration of observables used to construct the estimators of Figs. 4 and 5, see text for details

3 Systematic Studies

3.1 General Cases

On Fig. 3 are given the typical shapes of distributions (in color), compared to a Lorentzian with the same parameters (in gray), for $E_0 = \Gamma_0 = 1\,\text{MeV}$. We first recall that these distributions physically represent cross-sections. It seems quite natural that if the energy E-which corresponds in the case of the scattering of a neutron on a fragment at rest to the kinetic energy of the neutron—is zero then the resonance probability is also zero. At constant integral, if we bring the cross-section to zero for $E_0 = 0$ the "apparent" maximum of the function will therefore shift to low energies.[2]

Since taking into account the energy shift and the energy dependence of the width significantly modifies the distribution compared to a Lorentzian one, we present on Figs. 4 and 5 the evolution of these characteristic distributions as a function of the energies and widths of the resonances. In order to quantify this evolution, we define several estimators:

- the full width half maximum (FWHM), which is directly comparable to the Γ of the Lorentzian,
- the position of the maximum,
- the mean value,
- and a measure of the asymmetry.

Concerning this asymmetry, we decided not to take the usual Pearson's coefficient of skewness (or *skewness*[3]) because it was found to be numerically unstable due to the infinite integration. Given the functions studied (analytic and continuous with one maximum) we preferred a more graphical version (noted $\mathcal{A}$) which consists in measuring the "half"-widths at half maximum on the right Δx_r *and* left of the maximum Δx_l (see on Fig. 3 on the right), calculate the difference and normalize it to the sum (the *true* FWHM). Then if we call Δx_r and Δx_l the half-widths at half height on the right and on the left respectively, the respectively, so the asymmetry is written $\mathcal{A} = \frac{\Delta x_\text{r} - \Delta x_\text{l}}{\Delta x_\text{r} + \Delta x_\text{l}}$.

This estimator is therefore zero in case of a symmetrical distribution, positive if the distribution has a tail towards high energies and negative in the opposite case.

[2] Except for $\ell = 0$ states, see Sect. 3.2.

[3] Mathematically the moment of order 3 of the reduced centered variable $\gamma_1 = \text{E}\left[\left(\frac{X-\mu}{\sigma}\right)^3\right] = \frac{\mu_3}{\sigma^3}$ with $\mu_k = \text{E}\left[(X-\mu)^k\right] = \int_{-\infty}^{+\infty}(x-\mu)^k P(x)\text{d}x$ and $^2 = \mu_2$

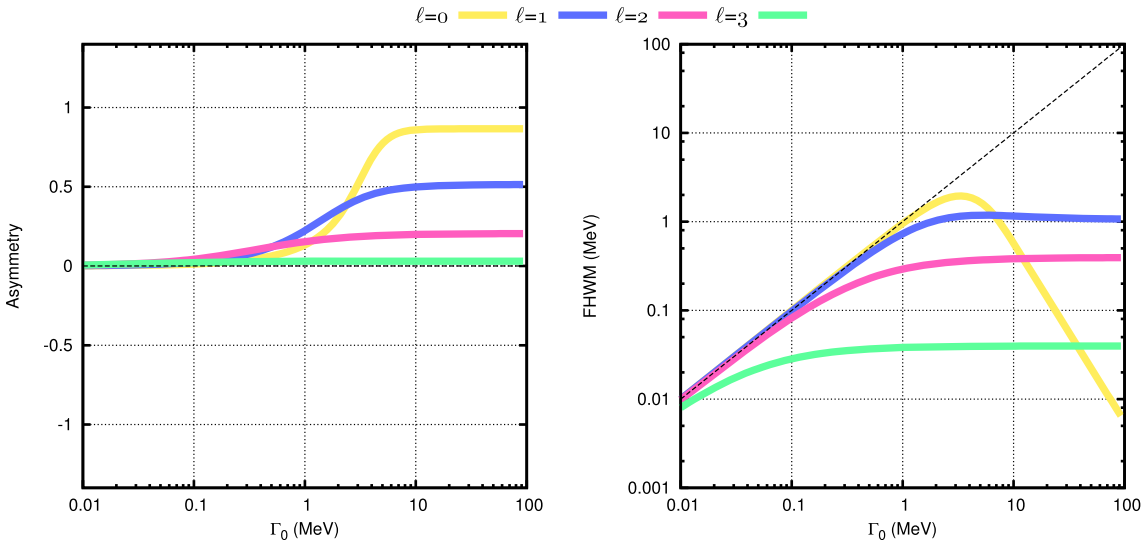

Fig. 4 Asymmetry (left) and FWHM (right) function of the intrinsic width of a Breit-Wigner centered at $E_0 = 1$ MeV for $\ell = 0$, 1, 2 and 3 (respectively yellow, blue, magenta and green). We consider here a $^{17}\mathrm{B}+n$ system. The dashed lines correspond to a Lorentzian function

A simple Lorentzian is symmetric (zero skewness) and its FWHM equals to Γ_0. The position of the maximum and the mean are both equal to E_0. All these cases are represented in black dashed lines on Figs. 4 and 5. On our illustrations the axes are in MeV and we will take as reference a distribution with $E_0 = \Gamma_0 = 1$ MeV. We could also have put axes (E/E_0, Γ/Γ_0 etc) since these distributions can be scaled by theses factors. Note that the result is not *necessarily physical* since certain combinations/values of E_0, Γ_0 and ℓ are not relevant (see Sect. 3.3).

Let's start with the left panel of Fig. 4 i.e. the asymmetry function of the intrinsic width for a resonance at $E_0 = 1$ MeV for different ℓ. This one is always positive (or almost zero for very low Γ_0) because the distribution presents a tail always towards high energies. The latter tends to move away from zero for $\Gamma_0 < E_0$ to saturate at a at values depending on the ℓ (the lower ℓ is the lower the saturation value). Consequently, on the right panel of Fig. 4 which shows the real width as a function of the intrinsic width, we observe a saturation of the real width when the intrinsic width increases. Therefore, *even if experimentally our resolution is minimal, we are only marginally sensitive to large widths* and this is all the more true as ℓ gets larger, up to "saturation". We note that the distributions $\ell = 0$ have a different behavior, in particular the width is maximal around $\Gamma_0 = E_0$ and decreases for width greater than E_0. This is not surprising given the particular nature of these resonances (see Sect. 3.2).

Concerning the evolution with the intrinsic energy of the resonance (at constant intrinsic width $\Gamma_0 = 1$ MeV), the different estimators are presented on Fig. 5. We first point out that these are not necessarily independent of each other. We note in the upper right corner that except for $\ell = 0$ the position of the maximum almost systematically coincides with E_0. The asymmetry (bottom left) is significant at low E_0 then tends to 0 at large E_0, which is the counterpart of the left panel of Fig. 4: it is equivalent to say that the larger the intrinsic width is compared to the energy of the resonance, the greater the asymmetry. This last observation has a direct consequence on the mean (top right), which is strongly shifted from the maximum to $E_0 \ll 1$ MeV. As for the FWHM, it is also away from 1 MeV in the same range of conditions.

3.2 Virtual States

The previous systematic studies show that $\ell = 0$ states follow different trends with respect to $\ell > 0$ states. This behavior leads to what is called "virtual states" and is well explained by McVoy in his article [8]. To understand it, let's look at the evolution with energy of the widths of the states, as given by the Eq. (38). The latter shows the "penetrability" s_ℓ whose expression is recalled here:

$$s_\ell = \frac{2/\pi}{J^2_{\ell+1/2}(kR) + Y^2_{\ell+1/2}(kR)} \tag{50}$$

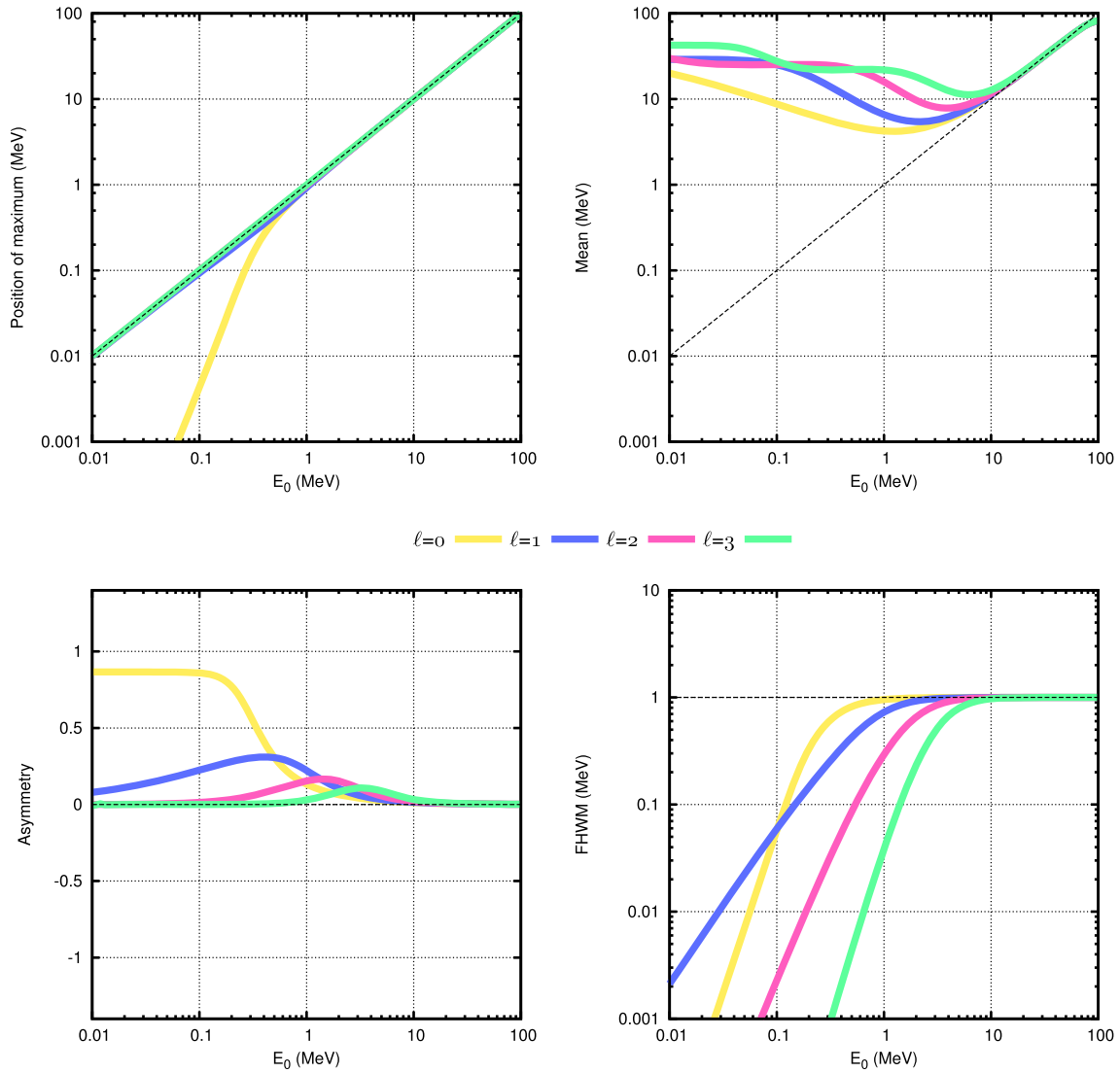

Fig. 5 Position of maximum (top left), mean energy (top right), asymmetry (bottom left) and FWHM (bottom right) function of energy of a Breit-Wigner of width $\Gamma_0 = 1$ MeV for $\ell = 0$, 1, 2 and 3 (yellow respectively, blue, magenta and green). We assume a $^{17}\mathrm{B} + n$ system

The Bessel functions $J_p(x)$ are written as:

$$J_p(x) = \sum_{m=0}^{\infty} \frac{(-1)^m}{m!\,\Gamma(m+p+1)} \left(\frac{x}{2}\right)^{2m+p} \tag{51}$$

with Γ the gamma function. The Bessel functions J_p and Y_p being related, for $p = \ell + 1/2$ with ℓ integer positive, by:

$$J_{-(\ell+1/2)}(x) = (-1)^{\ell+1} Y_{\ell+1/2}(x) \tag{52}$$

this implies that s_ℓ, and thus by extension the width Γ, evolves in $k^{2\ell+1}$. This is to be compared to the energy which varies in k^2 (Eq. (2)) and so for $\ell > 0$ the width decreases faster than the energy. In this case the state never overlaps the threshold, so there can not be any ambiguity as to whether it occurs above the threshold (a resonance) or below (a bound state). If $\ell = 0$ however, the width decreases *only* as the square root of the energy, so as the energy decreases, there will necessarily be an "overlap" threshold before it becomes a bound state. In some cases it is not clear whether the level is predominantly above or below the threshold, and to describe

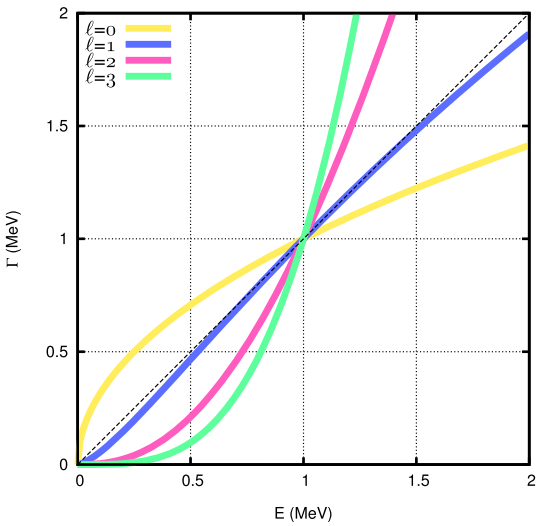

Fig. 6 Evolution of the width as a function of the energy of the resonance, for $\ell = 0, 1, 2$ and 3 (respectively yellow, blue, magenta and green). We consider here a $^{17}\mathrm{B} + n$ system with $E_0 = 1$ MeV. The $\Gamma = E$ case is depicted as a dotted black line

this situation the term "virtual" state is used. In order to illustrate this situation, we present the evolution of the width as a function of the energy, taking as reference the energy of the resonance $E_0 = 1$ MeV (from the Eq. (44) and with the same logic as the previous systematic analyses). We can see that only for $\ell = 0$ (in yellow) the width value is greater than the energy (in dotted line).

3.3 Width of Single-Particle Resonances

Experimentally the width of an independent particle state is often used, knowing the nature of the considered state, to deduce its spectroscopic factor. The link between the two can simply be seen in the definition, here simplified, of the reduced width as given in references [4,9]:

$$rrrCl \quad \gamma_{\ell,i} = \frac{\hbar}{\sqrt{2\mu R}} \int \phi_\ell^\star \chi_i dS \tag{53}$$

where : dS surface element at $r = R$

ϕsurface component of the internal wave function

χ_i internal eigenfunction, for an given energy E_i (54)

The surface component corresponds to what must be multiplied with the radial wave function u_ℓ to obtain the total wave function ψ:

$$\psi = \sum_\ell u_\ell \, \phi_\ell = \sum_i A_i \, \chi_i \tag{55}$$

Quantitatively, it appears here because γ_ℓ, if we refer to Eq. (37), shows the derivative according to r of the wave function. Note that in expression (55) presented here the summation is simplified on ℓ but, in particular R-matrix formalism [4,9], one must take into account all the quantum numbers of the input channels of the reaction (j, l, J, etc).

We clearly see in this expression that the spectroscopic factor C^2S, is directly connected to the observed width. Schematically:

$$C^2S = \sigma_{\ell,\mathrm{exp}}/\sigma_{\ell,\mathrm{theo}} \tag{56}$$

with σ_ℓ the cross-section of interest, $\sigma \propto \|\phi\|^2$, experimental and theoretical respectively. So schematically again we can write $\phi_{\mathrm{exp}} = \sqrt{C^2S}\,\phi_{\mathrm{theo}}$, which gives:

$$C^2S = \gamma_{\ell,\mathrm{exp}}/\gamma_{\ell,\mathrm{theo}} \tag{57}$$

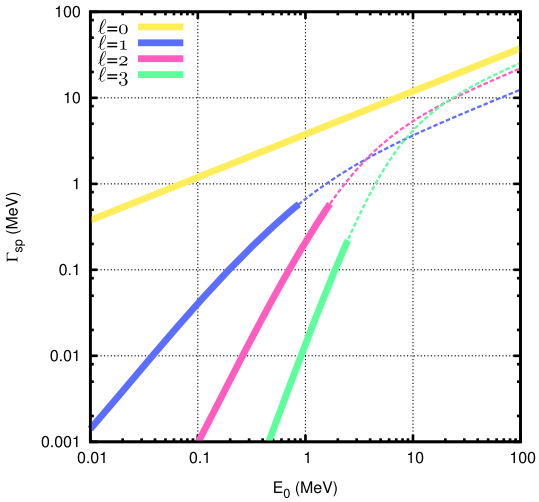

Fig. 7 Independent particle width as a function of energy of the resonance, according to the formalism of Bohr and Mottelson [10] and for $\ell = 0, 1, 2$ and 3 (respectively yellow, blue, magenta and green). We assume a $^{17}\mathrm{B} + n$ system. The dotted lines correspond to the case outside the necessary conditions for $kR < \ell^{1/2}$

Now to really evaluate the width of interest it is necessary to calculate the corresponding wave functions, for example from shell-model calculations, which is beyond this simple introduction. However, with a minimum of assumptions, notably a square well, it is possible to estimate these widths. Bohr and Mottelson then derive [10, p. 440]:

$$\Gamma_{sp} = \begin{cases} \frac{2\,\hbar^2}{\mu R^2}\, kR\, v_\ell\, \frac{2\ell-1}{2\ell+1} & \text{if } \ell > 0 \text{ and } kR < \ell^{1/2}, \\ \frac{2\,\hbar^2}{\mu R^2}\, kR & \text{if } \ell = 0 \end{cases} \tag{58}$$

A systematic study, using this formalism, is presented in Fig. 7 for the system $^{17}\mathrm{B} + n$, with the same conventions as in the Sect. 3, despite the limits of definition of (58), which explains why some values are "missing" (but presented here for information as a dotted line). We see in particular that the larger ℓ the smaller the width, which comes from the penetration factor effect.

3.4 Multineutron Resonances

The previous section presented two-body resonances and mainly fragment–neutron ones. Simple parametrizations for multi-body cases and three-body in particular are difficult because one of the assumption of the traditional R-matrix approach is the "absence or unimportance of all processes in which more than two product nuclei are formed" [4] which means that the theory cannot be used immediately for at least three-body decays. More complex modelization and theoretical calculations are thus necessary. One of the difficulties, both theoretical and experimental, is that several decay paths and combinations of them open. We should note however that some attempts have been done in particular when the decay is sequential [11,12], which in this case can be regarded as a two-step two-body process.

We would like to draw the attention on the fact that in absence of specific calculations authors generally extract the energy and the width of the "N-body" resonance using the parametrization described in the previous sections for two bodies. They sometimes also assume that N_n clustered neutrons participate to the resonance, as a multineutron "bound" system. In the authors' opinion, in absence of any other model, and as far as the resonance shape does not resemble a virtual one, the only acceptable parametrization to be used is $\ell = 0$ because this one does not exhibit any energy dependence on the position and the width. As shown also on Fig. 8 (left) there is also no dependence in the width with the N_n neutrons clustered in a two-body resonance. Most of these systems close to the drip line present a substantial extension (halo, skin…) and a study of the effect of the radius r_0 (Fig. 8, right) also shows that $\ell = 0$ distributions are independent of this parameter. One would have to be careful with the exact meaning of this width which, even if the experimental resolution is taken into account to extract it, would be difficult to compare to theory. Probably the best approach will then be to produce from the theoritical approach the energy distribution and then fit it with the same $\ell = 0$ distribution.

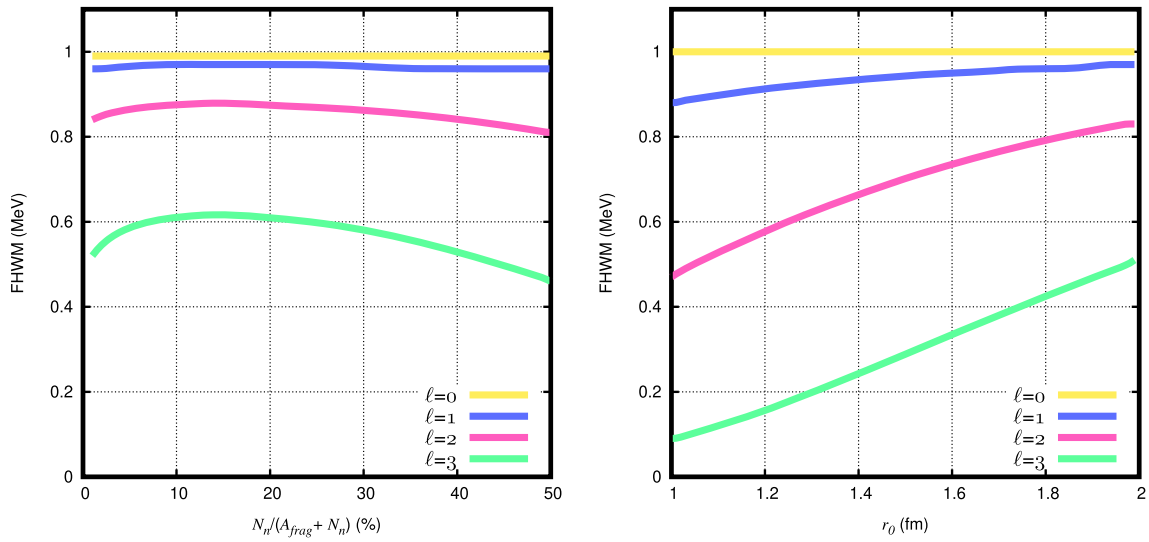

Fig. 8 Left: dependence of the width for two-body resonances, for different ℓ, function of the fraction of incident clustered neutrons. Right: same plot but function of the r_0 parameter used to calculate the fragment radius

4 Conclusion

We presented in this paper a series of simple calculations to describe two-body resonances and alike. These results represent a parametrization often used to extract the properties of resonances measured experimentally, in particular for nuclei far from stability or beyond drip-lines. The main purpose of this article was to put then in perspective and illustrate the evolution of the measurable properties with their intrinsic parameters, in particular to the attention of physicists studying resonance properties and comparing them to theoretical models.

Declarations

Conflict of interest The authors declare no competing interests.

Author Contribution The author is the only contributor.

References

1. N. Austern, Direct nuclear reaction theories, in *Interscience Monographs and Texts in Physics and Astronomy* (Wiley-Interscience, 1970). 30620
2. J.M. Blatt, V.F. Weisskopf, *Theoretical Nuclear Physics* (Wiley, New York, 1984)
3. G.R. Satchler, *Introduction to Nuclear Reactions*, 2nd edn. (Oxford University Press, Oxford, 1990)
4. A.M. Lane, R.G. Thomas, *R*-matrix theory of nuclear reactions. Rev. Mod. Phys. **30**, 257–353 (1958). https://doi.org/10.1103/RevModPhys.30.257
5. P. Descouvemont, D. Baye, The *R*-matrix theory. Rep. Prog. Phys. **73**(3), 036,301 (2010)
6. F. Gunsing, in *Joliot-Curie School* (2014). https://ejc2014.sciencesconf.org/conference/ejc2014/pages/20150420_ejc2014_gunsing_1_2.pdf
7. B. Gough, *GNU Scientific Library Reference Manual—Third Edition*, 3rd edn. (Network Theory Ltd., 2009)
8. K. McVoy, Virtual states and resonances. Nucl. Phys. A **115**(3), 481–494 (1968). https://doi.org/10.1016/0375-9474(68)90741-0
9. A.M. Lane, Reduced widths of individual nuclear energy levels. Rev. Mod. Phys. **32**, 519–566 (1960). https://doi.org/10.1103/RevModPhys.32.519
10. A. Bohr, B. Mottelson, *Nuclear Structure* (World Scientific Publishing Company, Inc., London, 1998)
11. F.C. Barker, *R*-matrix formulas for three-body decay widths. Phys. Rev. **68**, 054,602 (2003). https://doi.org/10.1103/PhysRevC.68.054602
12. H.O.U. Fynbo, R. Álvarez-Rodríguez, A.S. Jensen, O.S. Kirsebom, D.V. Fedorov, E. Garrido, Three-body decays and *R*-matrix analyses. Phys. Rev. C **79**, 054,009 (2009). https://doi.org/10.1103/PhysRevC.79.054009